

Numbering-up Strategies for Microfluidics-Assisted Water Treatment Processes: Deterministic Lateral Displacement for the Removal of Bacteria and Parasites as a Case Study

Maria Anna Murmura, Valentina Biagioni, Stefano Cerbelli*

Dipartimento Di Ingegneria Chimica Materiali Ambiente, Sapienza Università di Roma - via Eudossiana 18 00184 Roma (Italy)

stefano.cerbelli@uniroma1.it

Microfluidic channels filled with spatially periodic arrays of impermeable obstacles have been proved successful for the size-based continuous separation of mesoscopic objects suspended in a buffer solution with unprecedented resolution. To date however, this technique - referred to as Deterministic Lateral Displacement (DLD) - has been implemented only for small volume samples, mainly for analytical purposes. In this article, we investigate the feasibility of the DLD separation technique for water purification from bacteria. The accurate numerical solution of the three-dimensional Stokes flow problem is used to establish the hydraulic resistance of several different geometries of the unit periodic cell. Results suggest that DLD-based microfilters resulting from numbering-up DLD microseparation units could provide sizeable flowrates and could prove competitive when compared to membrane-based modules.

1. Introduction

Besides the many practical advantages afforded by scaling down traditional processes to the micrometer and nanometer size, one of the fundamental novelties offered by microfluidics is the possibility of designing processes and device geometries based on either analytical or accurate numerical solutions of the mass and momentum transport equations, thus allowing for a detailed theoretical analysis of new transport regimes (see, e.g., Giona et al, 2009; Adrover et al, 2009; Cerbelli et al, 2017). In the last two decades, ever growing attention has been devoted to investigating the potential of micro- and nanotechnology-based processes for water treatment and remediation, sensing and detection of hazardous molecules and micro-organisms or pollution prevention (see Cloete, 2010; Bavasso et al., 2016, and therein cited references). A well-known example is the use of carbon nanotubes for the effective removal of pathogen agents such as *Escherichia coli* and *Staphylococcus aureus* from water (Srivastava et al, 2004). Despite the great potential for improved control and enhanced efficiency made possible by the scaled-down geometries of the equipment, many practical challenges have yet to be met and overcome in order to extend the domain of application of these techniques from the nanoliter-per minute range to more sizeable flowrates. The first and foremost among these challenges is the ability to build macroscopic structures that are constituted by thousands to million of replicas of the nano- or micro-scale unit (to be run in parallel), while maintaining the same degree of accuracy and suitable mechanical properties of the device as a whole. Therefore, to date, the bottleneck of this *numbering-up* approach is the development of micro-fabrication techniques that should allow a completely automatized fast production of arrays of microfluidic units arranged in compact volumes, by using cheap and readily available materials. In this respect, the most promising of these techniques is provided by 3D printing, whose resolution is swiftly reaching the tens-of-micrometers scale (Accardo et al., 2018). At this scale, new and unprecedented possibilities open up for moving a series of well established processes currently used only for analytical purposes to preparative, or even small production scale. In this work, we take one of these processes, referred to as Deterministic Lateral Displacement (henceforth DLD), as a prototypical case study to investigate quantitatively the numbering-up approach for water purification applications aimed at removing mesoscopic suspended objects such as bacteria and parasites to obtain drinkable water. The core of a DLD

device is constituted by a shallow channel with rectangular cross-section, filled with a periodic array of obstacles arranged along a planar Cartesian lattice. The axes of the obstacle lattice are tilted with respect to the channel walls (see the next Section for details). Experiments have demonstrated that size-based (label-free) separation of a population of suspended particles can be accomplished when the suspension is pushed by a pressure drop through the obstacle array (Huang et al, 2004). Specifically, the combined action of the deterministic drag on the particle by the surrounding fluid and the particle-obstacle interaction is such as to yield qualitatively different dynamics of individual particles. Particles whose size is below a critical value (critical radius) follow a zig-zag trajectory through the obstacle array with an average direction parallel to the carrier flow and, therefore, to the lateral walls of the channel. Particles with size above the critical radius are systematically displaced by the obstacles and follow a path whose average direction is parallel to the axis of the obstacle lattice (displaced mode). The critical size depends on the structure of the periodic laminar flow through the array, and therefore, ultimately, on the geometry (size and shape) of the obstacles as well as on the lattice vectors (length and mutual angle) defining the array (Cerbelli, 2012). We present a state-of-the-art theoretical/numerical investigation of optimized geometries that are specifically tailored to the case of bacteria removal from water and are aimed at minimizing the number of separation units. The results presented can therefore be considered as a preliminary attempt to fix the target to be met by 3D printing techniques for this type of application.

2. Device geometry and transport of finite-sized particles in Deterministic Lateral Displacement arrays

As pointed out in the Introduction, the core of a DLD microseparator is constituted by an array of impermeable obstacles arranged along a spatially-periodic two-dimensional Cartesian lattice. Cylindrical obstacles are here considered henceforth, even though different shapes have been investigated in order to reduce pressure drop and particle clogging (Louterback et al., 2010). The lattice is characterized by two linearly independent lattice vectors, say \mathbf{e}_1 , \mathbf{e}_2 , which can be orthogonal (tilted lattice) or askew (stretched lattice), as depicted in Figure 1. The characteristic length of the periodic cell, say $\ell = \|\mathbf{e}_1\|$ ultimately depends on the characteristic size of the suspension to be separated and can range from tens of micrometers down to the hundred of nanometer scale. The lattice angle, say θ_l , can be defined as the smallest angle between the lattice vectors and the average direction of the carrier flow.

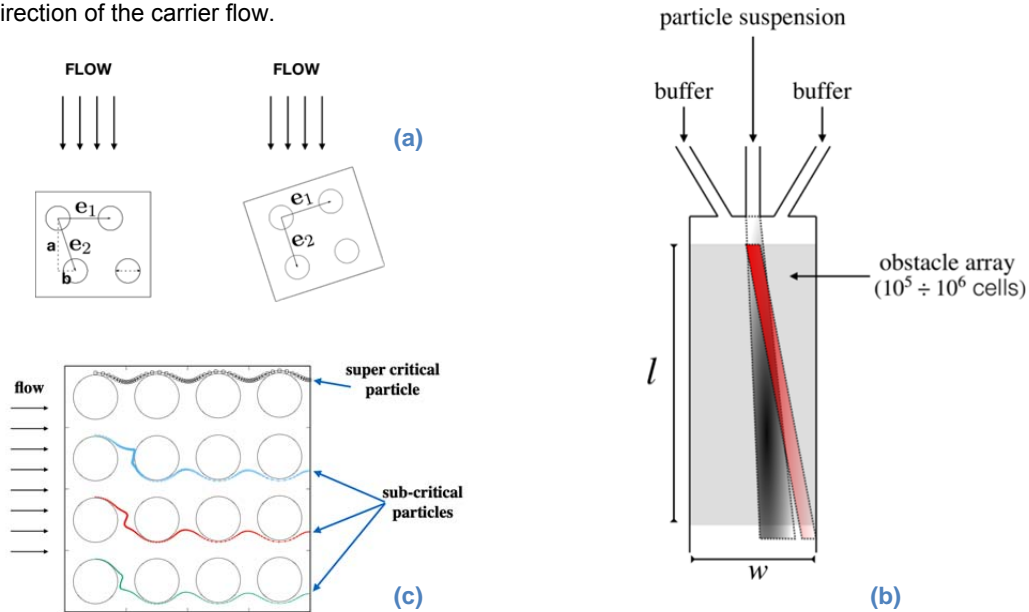


Figure 1: -(a) Typical obstacle lattice geometry for a stretched (left) and tilted (right) DLD arrays. In the stretched array the lattice angle is defined by the row shift fraction b/a ; -(b) Device configuration; -(c) Different particles trajectories for different particle sizes in the limit of vanishing diffusivity. Particles below the critical dimension (green, red, and blue) trace trajectories which possess the same average direction as the flow streamlines. Particles larger than the critical size are systematically deflected by the obstacle so that the average migration direction is equal to the lattice angle.

The obstacle lattice, which can count up to a million of elementary cells such as those depicted in Figure 1a, is hosted in a shallow rectangular channel whose typical length l , width w , and height h , are of order of $l \simeq 1\text{cm}$, $w \simeq 2\text{mm}$, and $h \simeq 0.5 \div 2\mu\text{m}$ (Figure 1b). A suspension of particles of different size is introduced through a narrow channel upstream the obstacle array, whereas lateral channels feed the device with fresh buffer solution so as to maintain the flowrate through the channel fixed to a prescribed value. Experiments (Huang et al 2004; Wunsh et al 2016) have demonstrated that, because of the interaction with the Stokesian drag of the surrounding fluid and of the obstacle-particle collisions, particles carried through the periodic structure migrate along different directions, which are at an angle with the direction of the carrier flow. Because the migration angle, say θ_p , depends on the particle radius as well as on the flowrate of the buffer solution, size-based sorting of the multi-dispersed particle suspension can be achieved, and particles of assigned size ranges can be collected at different locations of the device outlet.

Figure 1b schematically shows the typical transport properties exhibited by a mixture of particles of two characteristic dimensions as the suspension flows downstream the device. The mixture of suspended particles swiftly separates into two separate streams of smaller (grey-shaded) and bigger (red-shaded) particles, each characterized by an average direction and a dispersion bandwidth about the given direction, whose (root mean square) variance, say σ , increases as the square root of the distance travelled by the current from the injection point. The average migration angle θ_p increases with increasing particle dimension, and is included between the average flow direction and the lattice angle, $0 \leq \theta_p \leq \theta_l$. Theoretical models accounting for the flow structure, the particle-obstacle interaction, and the presence of Brownian (thermal) fluctuations have been proposed for addressing particle transport in these periodic structures (Cerbelli et al., 2013; Cerbelli, 2013; Cerbelli et al., 2015). The application of these models to typical device geometries and operating conditions used in DLD separations has been shown to consistently reproduce the transport phenomenology reported in the experiments. To the scopes of the present analysis, it is important to point out that the theoretical approach referred above rests upon a one-way coupling approximation of the two-phase transport problem, where the single-phase pressure driven flow of the carrier fluid is first solved as a stand-alone problem, and the transport of the suspended solution is evaluated *ex-post*, based on the structure of the laminar flow through the obstacle array (details can be found in the references cited above).

For values of the lattice angle that are commonly used in reported experiments (e.g. $\theta_l = \tan^{-1}(1/10)$, see Huang et al. 2004), the characteristic device length necessary to achieve an efficient separation can be estimated in the order of $10^3 \div 10^4$ rows of obstacles, with a characteristic pressure drop ranging from 10 to 10^2KPa for the lattice obstacle as a whole.

From the practical standpoint, DLD devices have proven successful for separating a variety of biological suspensions, ranging from the scale of tens to hundred nanometers (exosomes and viruses, see Wunsh et. al 2017; protein vesicles, see Smith et al., 2018) to micrometer-sized or even larger objects, such as, e.g., leukocytes (Inglis et al., 2011) and fungal spores (Inglis et al., 2010). The effect of particle deformability has also been considered (Quek et al., 2011). In the experiments reported in the literature, however, the separation operation is usually carried out for analytical purposes (i.e. in the spirit of separating for identifying) and, as such, it typically involves remarkably small sample volumes that can be treated in a reasonable process time, e.g. of the order of nanoliters per minute. In this respect, it is worth to observe that high throughput cannot be obtained in these devices by simply increasing the flowrate in that the large surface-to-volume ratio that characterize microfluidic lengthscales would imply large values of the pressure drop, which, in turn, might undermine the mechanical resistance of the structure, especially in those cases where soft lithography is used on amorphous polymeric material for generating the patterned structure (e.g. for PDMS-based devices). Thus, the strategy for increasing the total flowrate should rather be oriented towards a numbering-up approach, where a large number of devices (e.g. of order of thousand to a million) are run in parallel under the same values of the pressure drop that characterize analytical-type operations.

In the next Section, the feasibility of the numbering-up approach is discussed by taking the purification of water from bacteria and parasites as a case study and investigating a variety of device configurations for identifying the cell geometry that yields affordable flowrates with mechanically acceptable values of the pressure drop. Unlike the vast majority of previous studies, which assume a two-dimensional structure of the flow and target the streamline geometry as point of main interest, the focus here is on the hydraulic resistance, which inherently demands for a fully three-dimensional setting for the analysis. Incidentally, the results next described can also serve as a benchmark to establish the limits of the cell geometry within which a two-dimensional approach to predicting the flow geometry controlling particle kinematics can be considered physically grounded.

3. Fluid Dynamics and hydraulic resistance

Because of the characteristic size of the periodic cell ($\ell \approx 10^2 nm \div 10 \mu m$), the Reynolds number associated with DLD separation devices falls in the range $10^{-4} \leq Re \leq 1$. Thus, the flow through these structures can safely be assumed to be in the creeping (Stokes) flow regime, which implies linearity of the momentum balance equation and, in turn, strict proportionality between viscous forces and fluid velocity. Also, at short distances from the entrance of the obstacle array and/or from the lateral walls of the channel (practically, at distances of two to three units of the cell length), a spatially periodic structure of the flow with the same periodicity as the obstacle lattice can be enforced.

$$\nabla^2 \mathbf{v} = \nabla P (\nabla \cdot \mathbf{v} = 0) \quad (1)$$

By these properties, the flow structure can be predicted by solving the dimensionless Stokes problem on the three-dimensional periodic cell depicted in Figure 2. In Eq. (1), variables and operators have been made dimensionless by taking the cell edge ℓ , the volume-average velocity U over the periodic cell, and the typical viscous shear stress $\mu \ell / U$ as reference length, velocity, and pressure, respectively. Note that, unlike the classical reference pressure based on the density of kinetic energy used in the full Navier-Stokes problem, the latter reference value is the only appropriate scaling factor at vanishing values of the Reynolds number. Periodic conditions are enforced at opposite faces parallel to the xz and yz coordinate planes, whereas no-slip conditions are set at the surfaces at $z = 0$ and $z = \alpha$.

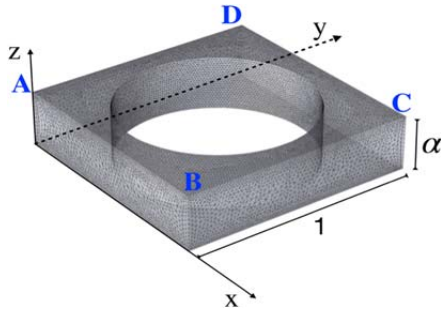


Figure 2: Example of dimensionless unit cell geometry and computational grid for the Finite Element discretization of the Stokes problem ($\alpha = 1/4$ for the case depicted).

Since the Cartesian Lattice is slanted by an angle θ_l with respect to the lateral walls of the channel, the pressure drops imposed along the x and y directions are set to $\Delta P_{AB} = \cos(\theta_l)$ and $\Delta P_{BC} = \sin(\theta_l)$, so that the average velocity direction of the carrier flow will form an angle θ_l with the positive direction of the x axis.

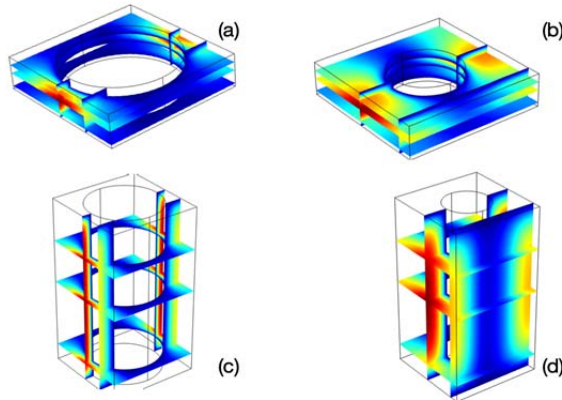


Figure 3: Dimensionless velocity magnitude at different values of the obstacle diameter and of the cell aspect ratio (see main text for details).

Figure 3 shows the effect of the obstacle diameter, D_o , and of the cell aspect ratio α on the magnitude of the local velocity. The scale of colors ranges linearly from zero (intense blue) to the maximum velocity (intense red).

The solution was obtained through a Finite-Element discretization of the Stokes problem defined above through the computational suite Comsol Multiphysics, by using order 5×10^5 degrees of freedom. The simulation results show that the region of high velocity becomes larger and larger when decreasing the obstacle diameter and at increasing aspect ratio. Quantitatively, the relationship between the dimensionless average velocity for a unitary (dimensionless) pressure drop through the cell is depicted in Figure 4a

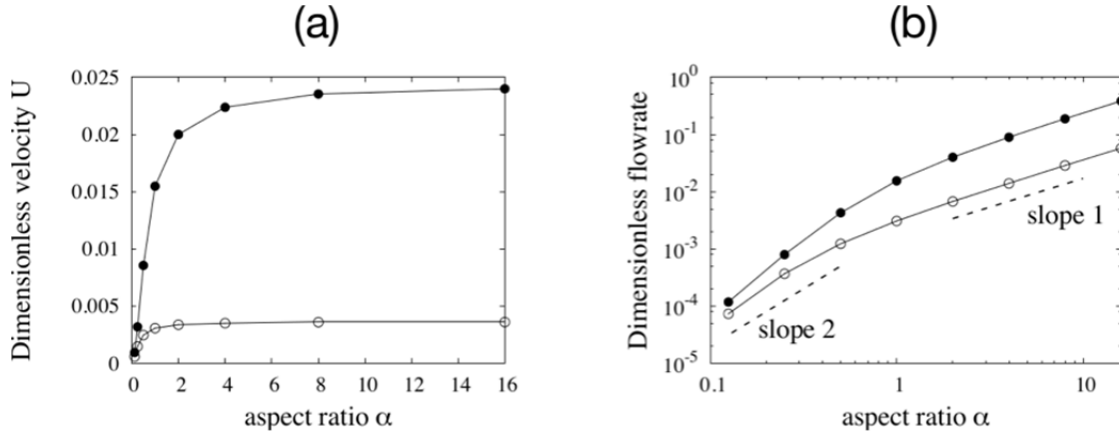


Figure 4: -(a): Volume-averaged dimensionless velocity vs α . Empty and solid symbols refer to post diameters D_o equal to 0.8 and 0.5, respectively. -(b) Dimensionless flowrate for the same cases as in Panel -(a).

For the larger diameter value ($D_o = 0.8$, empty symbols) the dimensionless velocity swiftly saturates towards a limiting value as the aspect ratio α is increased. In this regime, dissipation at the obstacle surface dominates over viscous friction due to the top and bottom walls of the cell. Consistently with this interpretation, in the case of a thinner obstacle ($D_o = 0.5$, solid symbols), the saturation limit is almost a decade bigger than the previous case, and is reached at larger α values ($\alpha \geq 5$). Figure 4b shows the dimensionless flowrate through the unit cell for the same cases depicted in Figure 4a. Here, the flow rate switches from a faster-than-quadratic dependence exhibited at low values of the aspect ratio to a linear dependence at larger α values, which settles down as the average velocity saturates towards a constant value. The dimensional counterpart of the dimensionless flowrates depicted in Fig 4b can be obtained once the cell size ℓ and the pressure drop per unit cell has been fixed. The first quantity is in turn related to the cutoff size of the object to be separated. If one targets an object dimension of $1\mu m$ and assumes a pressure drop of $20KPa$ over the elementary cell (as suggested by the experimental data in Huang 2004) then a three-dimensional array of DLD devices composed characterized by dimensionless cell parameters $D_o = 0.5$ and $\alpha = 2$ occupying an overall cross section of $5 \times 5cm^2$ could provide a total flowrate of the order of five litres per hour. This suggests that this technique could be implemented, e.g., for bacteria removal from water and could prove competitive when compared to membrane-based purification devices. In this respect, an accurate design of the post shape could prevent the occurrence of clogging, which is instead unavoidable in membrane modules thus limiting their use to a fixed lifetime.

4. Conclusions

A numbering-up strategy for moving DLD-based separation techniques from the analytical domain to the litre-per-hour flowrate has been investigated in the case of bacteria removal from water. 3D simulations of the Stokes flow problem for a variety of different cell geometries have been used to investigate the effect of the obstacle diameter and of the cell aspect ratio on the flowrate for an assigned pressure drop. It has been found that for fixed obstacle diameter the average dimensionless velocity saturates towards a limiting value when the aspect ratio increases over a critical value. Both the velocity limiting value and the critical aspect ratio depend on the obstacle diameter. An order-of-magnitude analysis based on these results suggests that the numbering-up approach could make DLD-based water filters competitive with membrane-based modules as far as the device lifespan is concerned. The economic feasibility of the method is instead tightly connected to the development of 3d printing techniques in that the current fabrication methods of these devices based on

lithography-etching techniques are not competitive with well established production processes of membrane-based modules.

References

- Accardo, A., Courson, R., Riesco, R., Raimbault, V., & Malaquin, L., 2018. Direct laser fabrication of meso-scale 2D and 3D architectures with micrometric feature resolution. *Additive Manufacturing*, 22, 440-446.
- Adrover, A., Cerbelli, S., Garofalo, F., & Giona, M., 2009. Convection-Dominated dispersion regimes in wide-bore chromatography: a transport-based approach to assess the occurrence of slip flows in microchannels. *Analytical Chemistry*, 19, 8009-8014.
- Al-Fandi, M., Al-Rousan, M., Jaradat, M. A., & Al-Ebbini, L., 2011. New design for the separation of microorganisms using microfluidic deterministic lateral displacement. *Robotics and computer-integrated manufacturing*, 27(2), 237-244.
- Bavasso I., Vilardi G., Stoller M., Chianese A., Di Palma L., 2016, Perspectives in nanotechnology based innovative applications for the environment, *Chemical Engineering Transactions*, 47, 55-60.
- Cerbelli, S., Garofalo, F., & Giona, M., 2015. Effective dispersion and separation resolution in continuous particle fractionation. *Microfluidics and Nanofluidics*, 19(5), 1035-1046.
- Cerbelli, S., Giona, M., & Garofalo, F., 2013. Quantifying dispersion of finite-sized particles in deterministic lateral displacement microflow separators through Brenner's macrotransport paradigm. *Microfluidics and nanofluidics*, 15(4), 431-449.
- Cerbelli, S., 2013. Critical dispersion of advecting-diffusing tracers in periodic landscapes of hard-wall symmetric potentials. *Physical Review E*, 87(6), 060102.
- Cerbelli, S., 2012. Separation of polydisperse particle mixtures by deterministic lateral displacement. The impact of particle diffusivity on separation efficiency. *Asia-Pacific Journal of Chemical Engineering*, 7, S356-S371.
- Cerbelli, S., Borgogna, A., Murmura, M. A., Annesini, M. C., Palocci, C., Bramosanti, M., & Chronopoulou, L., 2017. A Tunable Microfluidic Device to Investigate the Influence of Fluid-Dynamics on Polymer Nanoprecipitation. *Chemical Engineering Transactions*, 57, 853-858.
- Cloete, T.E., ed. *Nanotechnology in water treatment applications*. Horizon Scientific Press, 2010.
- Crevacore, E., Boccardo, G., Marchisio, D.L., Sethi, R., 2016. Microscale colloidal transport simulations for groundwater remediation *Chemical Engineering Transactions*, 47, 271-276.
- Devendra, R., & Drazer, G.i, 2012. Gravity driven deterministic lateral displacement for particle separation in microfluidic devices. *Analytical chemistry*, 84(24), 10621-10627.
- Giona, M., Adrover, A., Cerbelli, S., & Garofalo, F., 2009. Laminar dispersion at high Péclet numbers in finite-length channels: Effects of the near-wall velocity profile and connection with the generalized Leveque problem. *Physics of Fluids*, 21(12), 123601.
- Huang, L. R., Cox, E. C., Austin, R. H., & Sturm, J. C., 2004. Continuous particle separation through deterministic lateral displacement. *Science*, 304(5673), 987-990.
- Inglis, D. W., Lord, M., & Nordon, R. E., 2011. Scaling deterministic lateral displacement arrays for high throughput and dilution-free enrichment of leukocytes. *Journal of Micromechanics and Microengineering*, 21(5), 054024.
- Inglis, D. W., Herman, N., & Vesey, G., 2010. Highly accurate deterministic lateral displacement device and its application to purification of fungal spores. *Biomicrofluidics*, 4(2), 024109.
- Loutherback, K., Chou, K. S., Newman, J., Puchalla, J., Austin, R. H., & Sturm, J. C., 2010. Improved performance of deterministic lateral displacement arrays with triangular posts. *Microfluidics and nanofluidics*, 9(6), 1143-1149.
- Quek, R., Le, D. V., & Chiam, K. H., 2011. Separation of deformable particles in deterministic lateral displacement devices. *Physical Review E*, 83(5), 056301.
- Smith, J. T., Wunsch, B. H., Dogra, N., Ahsen, M. E., Lee, K., Yadav, K. K., ... & Papalia, J. M., 2018. Integrated nanoscale deterministic lateral displacement arrays for separation of extracellular vesicles from clinically-relevant volumes of biological samples. *Lab on a Chip*.
- Srivastava, A., Srivastava, O. N., Talapatra, S., Vajtai, R., & Ajayan, P. M., 2004. Carbon nanotube filters. *Nature materials*, 3(9), 610.
- Wunsch, B. H., Smith, J. T., Gifford, S. M., Wang, C., Brink, M., Bruce, R. L., ... & Astier, Y., 2016. Nanoscale lateral displacement arrays for the separation of exosomes and colloids down to 20 nm. *Nature nanotechnology*, 11(11), 936.